

This is the accepted manuscript made available via CHORUS. The article has been published as:

Structural transition and amorphization in compressed α - $\text{Sb}_{\{2\}}\text{O}_{\{3\}}$

Zhao Zhao, Qiaoshi Zeng, Haijun Zhang, Shibing Wang, Shigeto Hirai, Zhidan Zeng, and
Wendy L. Mao

Phys. Rev. B **91**, 184112 — Published 27 May 2015

DOI: [10.1103/PhysRevB.91.184112](https://doi.org/10.1103/PhysRevB.91.184112)

Structural transition and amorphization in compressed α - Sb_2O_3

Zhao Zhao,^{1,2,*} Qiaoshi Zeng,^{2,3,4} Haijun Zhang,^{5,1} Shibing

Wang,^{2,3} Shigeto Hirai,^{2,3,4} Zhidan Zeng,^{2,3,4} Wendy L. Mao,^{2,3,6}

¹*Department of Physics, Stanford University, Stanford, CA 94305, USA*

²*Stanford Institute for Materials and Energy Sciences,*

SLAC National Accelerator Laboratory, Menlo Park, CA 94025, USA

³*Department of Geological Sciences, Stanford University, Stanford, CA 94305, USA*

⁴*Center for High Pressure Science and Technology Advanced Research, Shanghai 201203, China*

⁵*National Laboratory of Solid State Microstructures and Department of Physics, Nanjing University, Nanjing 210093, China and*

⁶*Photon Science, SLAC National Accelerator Laboratory, Menlo Park, CA 94025, USA**

(Dated: April 24, 2015)

Sb_2O_3 -based materials are of broad interest in materials science and industry. High pressure study using diamond anvil cells shows promise in obtaining new crystal and electronic structures different from their pristine states. Here, we conducted *in-situ* angle dispersive synchrotron X-ray diffraction and Raman spectroscopy experiments on α - Sb_2O_3 up to 50 GPa with neon as the pressure transmitting medium. A first-order structural transition was observed in between 15 to 20 GPa, where the cubic phase I gradually transformed into a layered tetragonal phase II through structural distortion and symmetry breaking. To explain the dramatic changes in sample color and transparency, we performed first-principles calculations to track the evolution of its density of states and electronic structure under pressure. At higher pressure, a sluggish amorphization was observed. Our results highlight the structural connections among the sesquioxides, where the lone electron pair plays an important role in determining the local structures.

I. INTRODUCTION

Sb_2O_3 -based materials are of broad interest in materials science and industry^{1–24}. Because of their unique mechanical, chemical, and electronic properties, they are applicable as flame retardants for ceramics and fibers¹² and can be fabricated into non-linear optical devices^{13,25}. Sb_2O_3 belongs to the late XV group sesquioxides which also include As_2O_3 and Bi_2O_3 . Various polymorphs have been identified among sesquioxides^{4,7,8,10,26–33}. For Sb_2O_3 , three polymorphs α - Sb_2O_3 (senarmontite)^{4,7,8,10}, β - Sb_2O_3 (valentinite)⁷, and γ - Sb_2O_3 ³⁴ have been reported. Cubic α - Sb_2O_3 (space group $Fd\bar{3}m$) is the stable form at ambient pressure and temperatures below 570 °C, and can be viewed as a molecular crystal composed of Sb_4O_6 adamantanoid cages (see Fig. 1(a))^{4,7,8,10,35,36}. Orthorhombic β - Sb_2O_3 (space group $Pccn$) becomes more stable at ambient pressure and temperatures above 570 °C up to the melting point, and is composed of membrane rings built by SbO_3 pyramids⁷. γ - Sb_2O_3 is a quenchable (to ambient conditions) phase that is synthesized at high temperatures (300 to 500 °C) and high pressures (9 to 11 GPa), and this structure (see Fig. 1(d)) is constructed by cross linked Sb-O_4 units³⁴.

Close structural connections exist among late XV group sesquioxides. For example, c - As_2O_3 (arsenolite) has a similar structure to α - Sb_2O_3 , and β - Sb_2O_3 is isostructural to ε - Bi_2O_3 ^{4,6–8,10,37–40}. Interestingly, recent theoretical studies showed that many structures such as α - Sb_2O_3 , β - Sb_2O_3 and β - Bi_2O_3 could be derived from a defective fluorite structure through symmetry breaking and local distortions^{19,41}. Pressure is a powerful tool in tuning atomic distances and arrangements,

and thus may enable studies on the connections between these structural models.

Previous studies have identified a number of pressure-induced structural transitions and amorphization in Bi_2O_3 , Sb_2O_3 , and As_2O_3 ^{18,20,34,41,42,44–48}. For α - Sb_2O_3 , a high pressure study combining X-ray Diffraction (XRD) and Raman experiments with *ab-initio* calculations²⁰ reported several interesting results on it. It demonstrated two iso-structural transitions occurred at 3.5 GPa and 10 GPa. Furthermore, it suggested α - Sb_2O_3 would transform into a tetragonal structure above 25 GPa²⁰. However, this transition was not verified by their experiments due to a lack of pressure. Therefore, experiments at higher pressure are needed to study potential phase transitions in α - Sb_2O_3 and explore the relationship among different structures in XV group sesquioxides.

In this work, we conducted *in-situ* XRD and Raman spectroscopy measurements to ~ 50 GPa on α - Sb_2O_3 with neon as the pressure medium. We identified a first-order structural transition from the initial cubic structure to a tetragonal structure at ~ 15 GPa and further discovered an amorphous phase at higher pressure. In addition, we performed *ab-initio* calculations on the electronic states of the two phases and the results shed light on the as-observed sharp changes in sample transparency under pressure.

II. EXPERIMENTAL AND THEORETICAL METHODS

Near stoichiometric (purity greater than 99 %) cubic α - Sb_2O_3 powder was purchased from Sigma-Aldrich

(Product no. 230898 and Lot no. MKBJ9063, purity tested by XRD and titration by iodine). Symmetric Diamond Anvil Cells (DACs) with 300- μm culets size were used to generate high pressure. Tungsten gaskets were pre-indented to 20 GPa and a 150- μm diameter sample chamber was drilled in the center of the indent. *In-situ* angle dispersive XRD data was collected at beamline 16 BM-D of the Advanced Photon Source (APS), Argonne National Laboratory (ANL) and at beamline 12.2.2 of the Advanced Light Source (ALS), Lawrence Berkeley National Laboratory (LBNL). The X-ray wavelength was 0.4246 Å. The Rietveld refinement of the integrated powder diffraction patterns was performed using GSAS-EXPGUI package⁴⁹. Raman spectra were collected using a Renishaw inVia micro Raman system with a 514 nm laser excitation line in the Extreme Environments Laboratory, Stanford University. Neon was used as the pressure transmitting medium for both the XRD and Raman measurements. Gas loadings were performed at GSECARS, APS, ANL and Extreme Environments Laboratory.

For the first-principles calculations, the Vienna *ab-initio* Simulation Package (VASP)^{50,51} was employed with the framework of Perdew-Burke-Ernzerhof type⁵² generalized gradient approximation of density functional theory⁵³. The projector augmented wave⁵⁴ pseudo-potential was used for all the calculations. The kinetic energy cutoff was fixed at 450 eV. The lattice parameters were directly taken from the Rietveld refinement. The theoretical atomic positions are electronically relaxed based on the experimental atomic positions.

III. RESULTS AND DISCUSSION

A. *In-situ* X-ray diffraction experiments

Experimental XRD patterns are shown in Fig. 2(a). A first-order structural transition from cubic phase I to tetragonal phase II occurred at ~ 15 GPa, where the cubic structure could not be used to fit higher pressure patterns. This transition was characterized by the asymmetric broadening of phase I peaks, and the appearance of a new peak from phase II at 2θ near 8.7° (d -spacing ~ 1.4 Å). The largest d -spacing (111) reflection from phase I disappeared completely when the transition was complete at ~ 20 GPa. At pressure higher than 37 GPa, the sample started to lose its long-range order and an amorphous component was observed (Fig. 2(b)). Decompression experiment shows the amorphous phase is quenchable.

At ambient pressure, the unit cell volume we measured was $1383.5(1)$ Å³, agreeing well with previous data^{7,20}. The volume as a function of pressure is presented in Fig. 3. The Fig. 3 inset shows the evolution of the cell parameters under pressure. The cell parameters a and c in the tetragonal phase II (4 Sb₂O₃ per unit cell) are multiplied by different factors to match the unit cell volume

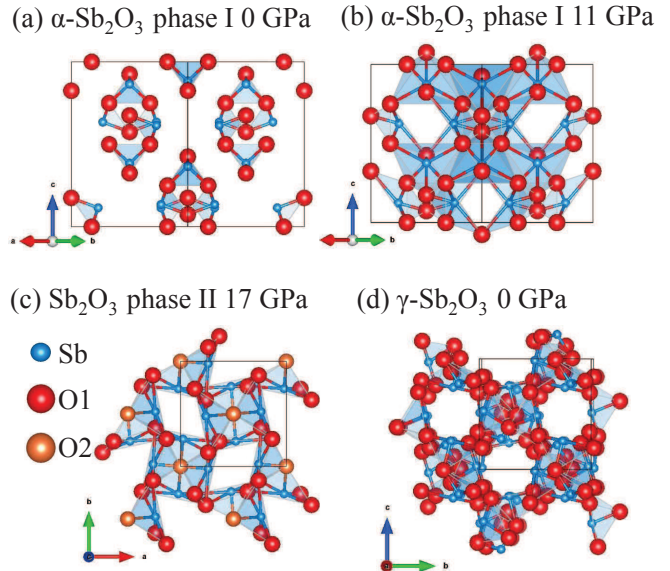


FIG. 1. (Color online) Structures of (a) α -Sb₂O₃ phase I at ambient conditions and (b) α -Sb₂O₃ phase I at 11 GPa (c) Sb₂O₃ tetragonal phase II at 17 GPa, with two O sites (d) γ -Sb₂O₃ at ambient conditions, from Ref [34], where there are six O sites.

of cubic phase I (16 Sb₂O₃ per unit cell). In the previous study, the (111) reflection disappeared completely at 17.9 GPa, and the (400) became much broader being in fact was composed of two close peaks (002) and (220) from phase II, see Fig. 4(b). It is worth noting that its calculated volume is quite different from our experimental data, off by 2 to 3 %, see Fig. 3. The different enthalpies from experimental volumes and theoretical volumes may explain why the first-order structural transition occurred at a lower pressure experimentally (15 to 20 GPa) than predicted (i.e. above 25 GPa)²⁰. Also, there may lie a region where phase I and phase II coexist.

For phase I, we fit our data to a third-order Birch-Murnaghan equation of state (BM-EOS) with fixed experimental $V_0 = 86.47(1)$ Å³ per formula, and obtained $B_0 = 27.4(7)$ GPa and $B' = 7.7(3)$, though the lack of data points in phase I may prevent the EOS determination of the three isostructural phases shown by the previous study²⁰. The relatively large B' value indicates a large change in compressibility with pressure. For phase II, we used a second-order BM EOS due to the limited number of data points, and the result was $V_0 = 79.3(5)$ Å³ per formula and $B_0 = 73(3)$ GPa (B' fixed at 4). We expect strong structural connections between the phase I and phase II structures due to following observations: (1) most of the XRD peaks in phase I continuously evolve into phase II, (2) the volume drop from phase I to phase II is relatively small and (3) the a of phase I splits into the a and c of phase II.

TABLE I. Experimental crystallographic information for phase I and phase II from GSAS-EXPGUI. Note that the atomic positions for $Fd\text{-}3m$ come from Origin choice I.

Pressure (GPa)	Space group	Volume (\AA^3)	Cell parameters		Atom	Experimental atomic positions		
			a (\AA)	c (\AA)		x	y	z
Phase I	Cubic	1383.5(1)	11.143(1)	–	Sb (32e)	0.885(1)	0.885(1)	0.885(1)
Ambient	$Fd\text{-}3m$ (227)	Z = 16			O (48f)	0.179(1)	0	0
Phase I	Cubic	1141.6(1)	10.451(2)	–	Sb (32e)	0.877(1)	0.877(1)	0.877(1)
10.7 GPa	$Fd\text{-}3m$ (227)	Z = 16			O (48f)	0.191(1)	0	0
Phase II	Tetragonal	267.9(1)	7.223(1)	5.135(2)	Sb (8e)	0.020(1)	0.257(1)	0.262(2)
17.2 GPa	$P\text{-}42_1c$ (114)	Z = 4			O (8e)	0.342(4)	0.259(6)	0.442(5)
					O (4c)	0	0	0.324(12)

TABLE II. Theoretical atomic positions for phase I and phase II from VASP. The cell parameters are fixed as the experimental values in Table 1.

Pressure (GPa)	Space group	Volume (\AA^3)	Cell parameters		Atom	Theoretical atomic positions		
			a (\AA)	c (\AA)		x	y	z
Phase I	Cubic	1383.5	11.143	–	Sb (32e)	0.883	0.883	0.883
Ambient	$Fd\text{-}3m$ (227)	Z = 16			O (48f)	0.190	0	0
Phase I	Cubic	1141.6	10.451	–	Sb (32e)	0.874	0.874	0.874
10.7 GPa	$Fd\text{-}3m$ (227)	Z = 16			O (48f)	0.199	0	0
Phase II	Tetragonal	267.9	7.223	5.135	Sb (8e)	0.023	0.267	0.245
17.2 GPa	$P\text{-}42_1c$ (114)	Z = 4			O (8e)	0.310	0.230	0.518
					O (4c)	0	0	0.263

To fit the diffraction patterns of phase II, we tried a number of different structural models in the sesquioxides, such as $c\text{-As}_2\text{O}_3$, $\beta\text{-Sb}_2\text{O}_3$, $\gamma\text{-Sb}_2\text{O}_3$, $\beta\text{-Bi}_2\text{O}_3$ (similar to $\epsilon\text{-Bi}_2\text{O}_3$) and $m\text{-As}_2\text{O}_3$ (claudetite), and the best fit came from the $\beta\text{-Bi}_2\text{O}_3$ structure. Fig. 4 shows the Rietveld refinements for phase I and phase II. The inset of Fig. 4(b) shows the splitting of (002) and (222) in tetragonal structure that could not be described by a single reflection (400) in cubic structure. All of the Rietveld refinements were performed without adding preferred orientation. Table I shows the experimental crystallographic information for phase I and phase II from GSAS-EXPGUI. Table II shows the theoretical atomic positions that are electronically relaxed based on the experimental atomic positions (the lattices are fixed at experimental values). Notice that the experimental and theoretical positions of Sb agree well with each other, while the O positions are slightly different. This is because O is a relatively weak X-ray scatter when compared to Sb, which then results in larger uncertainty in determining the atomic position of O during Rietveld refinement.

In $\alpha\text{-Sb}_2\text{O}_3$ phase I (from ambient to 15 GPa), the coordination of Sb-O increased from 3 to 6. As seen in Fig. 1(a) and Fig. 1(b), phase I changes from Sb_4O_6 cages (Sb-O_3 tetrahedra) at ambient pressure to a layered network (Sb-O_6 with 3 in-plane O and 3 out-of-plane O) at high pressure²⁰. For phase II, the $\beta\text{-Bi}_2\text{O}_3$ type structure has two crystallographically inequivalent O sites: O1 links with two Sb at an angle close to 110° while O2 connects with 2 Sb almost linearly; for Sb, it forms Sb-O_5

pyramid-like polyhedra, where there are 4 in-plane O1 and 1 out-of-plane O2. Noticeably, in both phase I and phase II, the out of plane O atoms always stay on one side of the O plane, consistent with that the fact that the lone 4s electron pair of Sb occupies the other side and do not form bonding with O. This further supports the role of the lone electron pair in determining local coordinations shown in previous calculations^{19,41}.

This phase II structure (Fig. 1(c)) bears some similarities to the previously reported $\gamma\text{-Sb}_2\text{O}_3$ structure (Fig. 1(d)). In particular, The oxygen sites in $\gamma\text{-Sb}_2\text{O}_3$ can be approximated into two categories similar to those in Sb_2O_3 phase II. However, their structures are differences in following aspects (1) $\gamma\text{-Sb}_2\text{O}_3$ ($P2_12_12_1$, Z = 8) has a lower symmetry and lower coordination numbers than the tetragonal phase II ($P\text{-}42_1c$, Z = 4) phase and (2) $\gamma\text{-Sb}_2\text{O}_3$ has more cryptographically different Sb and O sites, e. g. 6 exact oxygen sites. These structural variations are strongly related to the different experimental conditions. $\gamma\text{-Sb}_2\text{O}_3$ was obtained at slightly lower pressures (9 to 11 GPa) and much higher temperatures (300 to 500 $^\circ\text{C}$). It is expectable that higher kinetic energies at elevated temperatures may further break the bonding symmetry and increase local distortions.

Above 31 GPa, a sluggish amorphization was observed. For instance, the (211) of phase II 2θ near 8.8° gradually became very broad while reflections (220) and (002) at near 9.5° became much weaker. At the highest pressure of 47.4 GPa in this study, the diffraction pattern (Fig. 2(b)) clearly shows a large amount of amorphous component.

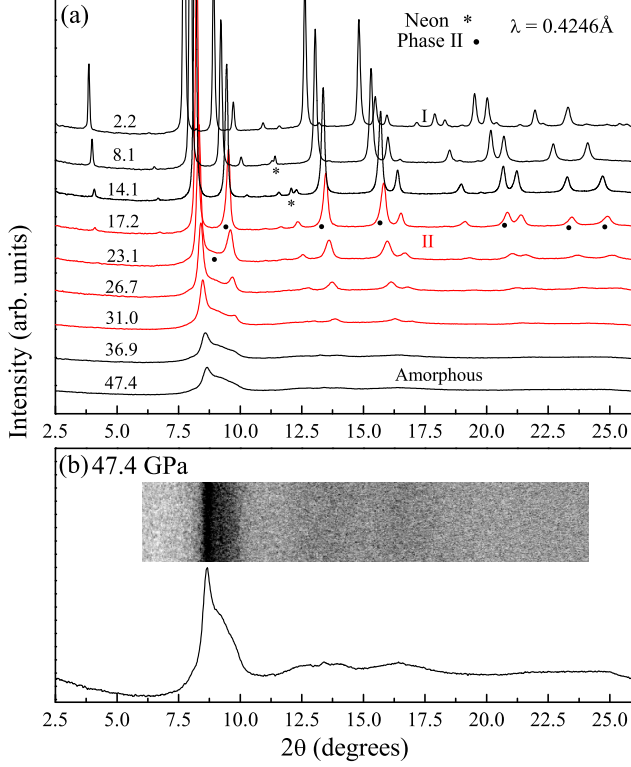


FIG. 2. (Color online) (a) Representative XRD patterns collected during compression up to 47.4 GPa with X-ray wavelength of 0.4246 Å. The numbers represent pressures in unit of GPa. (b) XRD pattern at the highest pressure shows the lack of long range order, insert is the cake 2D image.

B. Raman spectroscopy measurements

To probe the changes of phonon modes during this structural transition and find proof for amorphization, we performed Raman experiments with a low laser power of 3 mW up to 48.6 GPa (Fig. 5). Although 3 mW is already very low, to rule out possible heating effects from the laser we repeated the Raman experiments with a much lower laser power of 1 mW up to 50.2 GPa and observed the same behavior.

Each peak was fit to one Voigt function using PEAKFIT and the results are shown in Fig. 6. Below 15 GPa, our data agreed with the previous study that demonstrated the two iso-structural transition at ~ 3.5 GPa and 10 GPa²⁰, where the slopes of pressure dependence for some modes changed strongly, i.e. see the E_g mode in Fig. 6(d). Above 15 GPa, our study suggested the occurrence of a first-order structural transition due to following observations: (1) In between 15 to 30 GPa, the slopes of pressure dependence, i. e. the E_g mode ~ 120 cm^{-1} shifted with pressure (See Fig. 6(d)), E_g mode ~ 300 cm^{-1} , and F_{2g} modes ~ 360 cm^{-1} (see Fig. 6(c)) varied strongly. (2) At above 15 GPa, E_g mode ~ 125

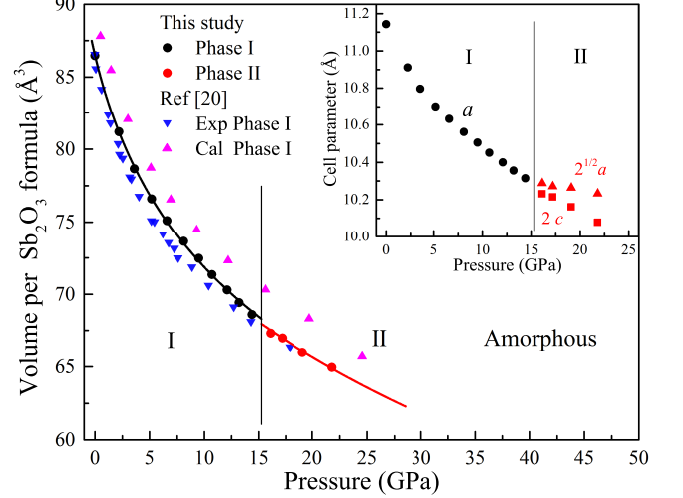


FIG. 3. (Color online) Pressure versus volume for Sb_2O_3 . Phase I is shown in black and phase II in red. The inset shows the evolution of cell parameters under pressure. The cell parameters a and c in tetragonal phase II (4 Sb_2O_3 per unit cell) are multiplied by different factors to match the unit cell volume of cubic phase I (16 Sb_2O_3 per unit cell).

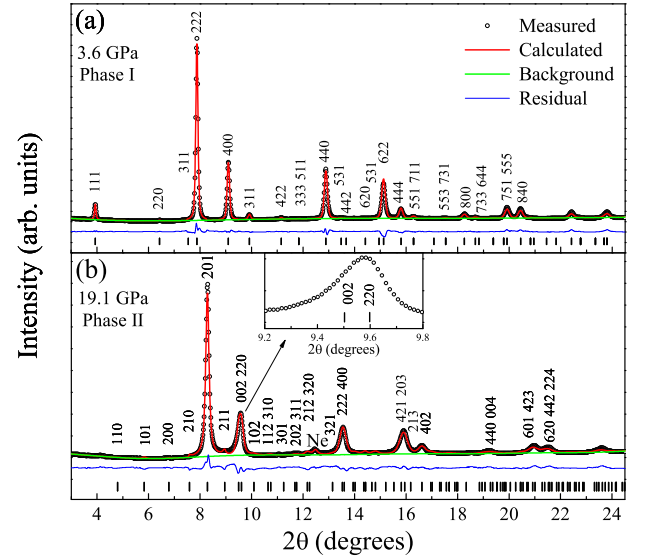


FIG. 4. (Color online) Rietveld refinement profiles for (a) phase I at 3.6 GPa (b) phase II at 19.1 GPa.

cm^{-1} and A_{1g} mode ~ 275 cm^{-1} exhibited increasing full width half maximum (FWHM) with pressure. At above 30 GPa, obvious splitting of them could be observed (See Fig. 6(a)). Linear extrapolations of these new peaks indicate that they may appear at ~ 20 GPa and 30 GPa. Further increase in pressure resulted in strong decrease in peak intensities. At the highest pressure 48.6 GPa, no Raman peaks were observed.

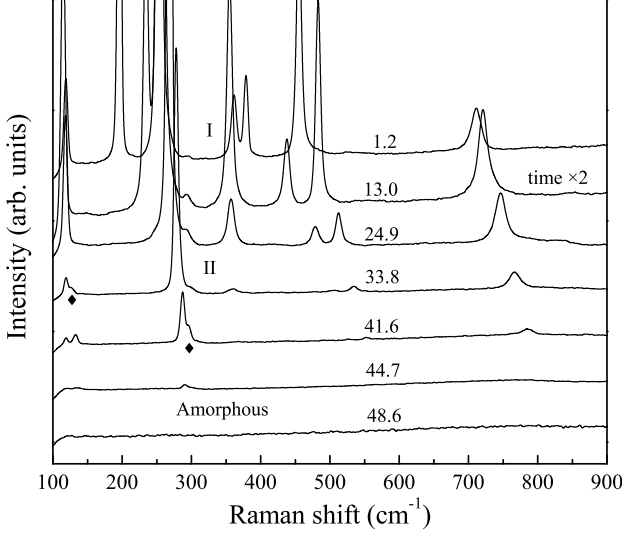


FIG. 5. (Color online) Representative Raman spectra collected during compression. The diamonds symbol indicates new peaks from phase II. The numbers represent pressures in unit of GPa.

C. Optical observations and first-principles calculations

Under pressure, the color of sample evolved from white to yellow, then to red, and finally to completely opaque, see Fig. 7, as were repetitively observed in all our experiments. Such dramatic changes suggest possible metalization and prompt us to investigate the electronic band structure and density of states (DOS). The DOS results from first-principles calculations at four representative pressures are shown in Fig. 8.

At ambient conditions, α - Sb_2O_3 is a semiconductor with an optical band gap of about 4 eV^{4,5}. For ambient condition α - Sb_2O_3 , our calculated indirect-band-gap is 3.0 eV, about 25 % smaller than the experimental value, which is not surprising because first-principles calculations tend to underestimate the band-gap. Visible light covers the range from violet (400 nm, 3.1 eV) to red (700 nm, 1.8 eV), so it is reasonable that the sample looked transparent to white light due to a lack of absorption in this region.

At 10.7 GPa, the band-gap decreases to about 2.2 eV. Since visible light with higher energies will be largely absorbed, the sample would appear yellow. At higher pressure, phase II remains semiconducting with a much smaller band-gap: 0.4 eV at 17.2 GPa and 0.2 eV at 21.8 GPa, which may explain why the color of the sample turned red and opaque finally. In contrast, the previous study assuming there was no first-order structural transition calculated the band-gap to be as large as ~ 3.8 eV

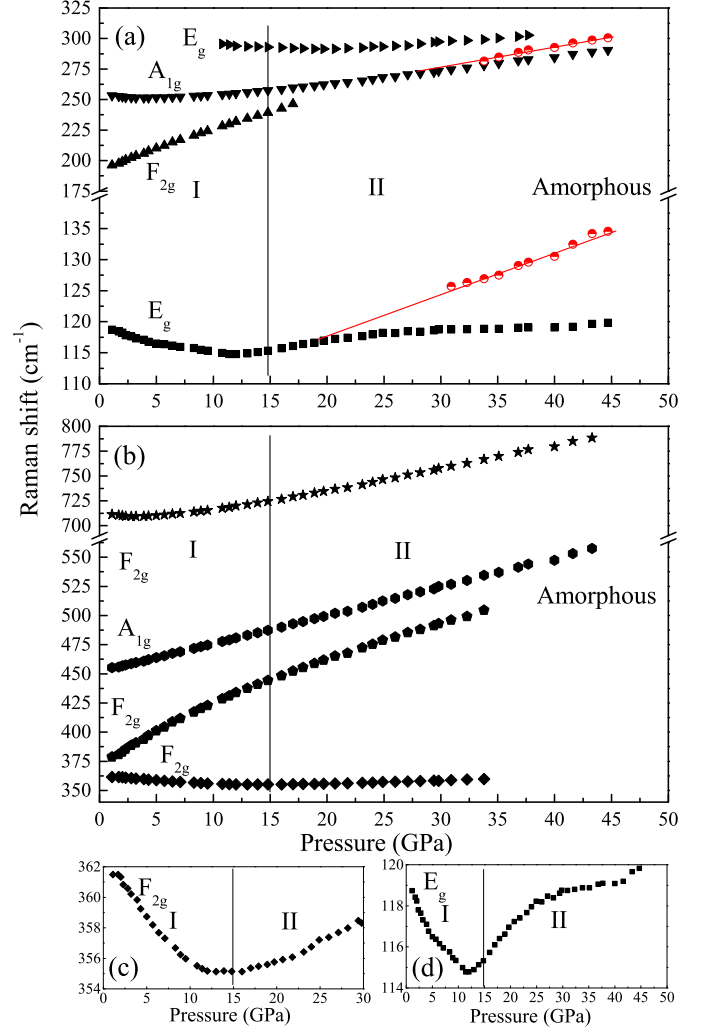


FIG. 6. (Color online) Evolution of Raman modes with pressure. Raman modes between (a) 110 to 325 cm^{-1} (b) 325 to 800 cm^{-1} . New modes from phase II are marked by red and linearly extrapolated to lower pressures. (c) and (d) show detailed changes of the F_{2g} and E_g modes.

at 20 GPa²⁰. At higher pressure, the featureless Raman spectra and total opacity at ~ 50 GPa suggest a possible metallic, amorphous phase of Sb_2O_3 .

The band structures at four representative pressures ambient pressure, 10.7 GPa, 17.2, and 21.8 GPa are shown in Fig. 9. The results for phase I at ambient and 10.7, see Fig. 9(a)-(b), clearly shows the indirect feature of its electronic structure, where the indirect-band-gap lies in between Γ of the conduction band and L of the valence band. Remarkably, upon entering phase II (Fig. 9(c)), the band structure shows a direct feature. The direct-band-gap of phase II is located at Γ and this direct feature is well maintained upon further compression (Fig. 9(d)).

Our high pressure study on α - Sb_2O_3 provides exper-

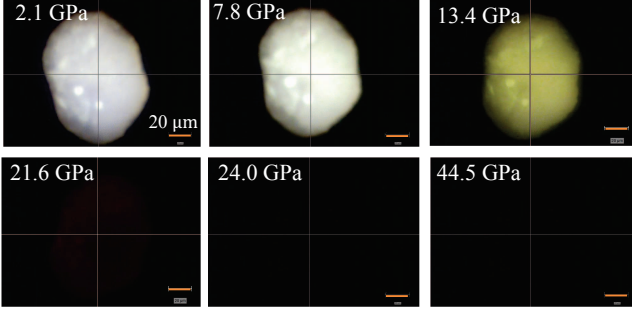


FIG. 7. (Color online) Optical photomicrographs of sample in transmitted light.

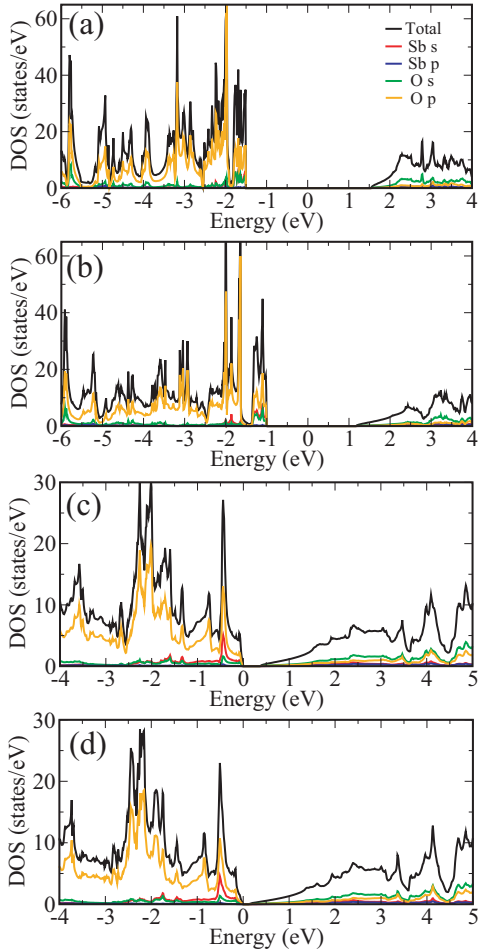


FIG. 8. (Color online) Calculated DOS of phase I at (a) ambient pressure and (b) 10.7 GPa, and phase II at (c) 17.2 GPa and (d) 21.8 GPa.

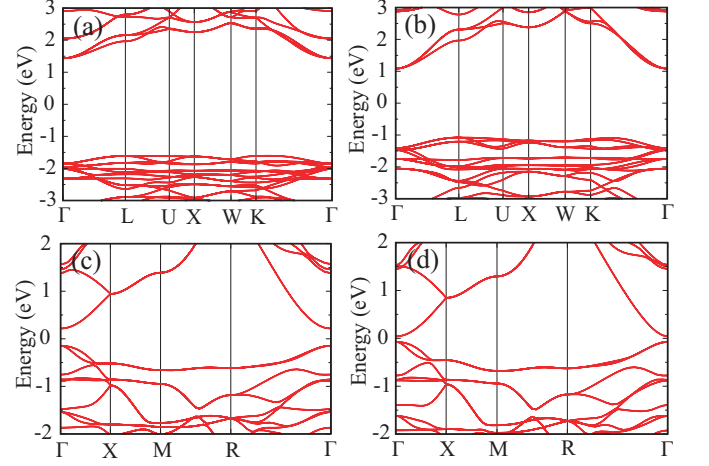


FIG. 9. (Color online) Calculated band structure of phase I at (a) ambient pressure and (b) 10.7 GPa, and phase II at (c) 17.2 GPa and (d) 21.8 GPa.

imental evidence for transitions from the cubic phase I to a tetragonal phase II and eventually to an amorphous phase. These findings shed light on the structural relationships between these phases during compression. It is noteworthy that one theoretical work have proposed a $<100>$ Sb_2O_3 structure (equivalent to the phase II we identified) and showed it was not dynamically stable without external pressure¹⁹. Here, we for the first time experimentally demonstrated that this structure becomes can be stabilized under pressure. This further suggests that pressure can serve as an important tool in testing the theoretical models among various sesquioxide polymorphs.

Furthermore, the observation of hollow cavities (large ordered vacancies) in the crystalline phases further supports the role of the lone electron pair in the $<111>$ and $<100>$ vacancy arrays, as implied from previous calculations on defective fluorite models^{19,41}. Phase I, composed of Sb_4O_6 cages, gradually transforms into a layered tetragonal phase II through local distortions and symmetry breaking, in which two crystallographically inequivalent O sites appeared. The physical properties (e.g. electric resistivity and optical conductivity) of these two phases are contrasting, resulting from large reduction in the electronic band-gap from a large-gap semiconductor (~ 4 eV, experimental) to a narrow-gap semiconductor (~ 0.5 eV, theoretical).

Another topic worth discussion is the amorphization of late XV group sesquioxides^{44,45,48,55}. Interestingly, the amorphous diffraction patterns we found at above 40 GPa (Fig. 2(a)) look similar to those of $c\text{-As}_2\text{O}_3$ at above 28 GPa⁴⁵ and the pattern for Sb_2O_3 glasses synthesized at ambient pressure²². They exhibited common features of a broad bump corresponding to the amorphous phase and a sharp peak at the large d -spacing. $\alpha\text{-Sb}_2\text{O}_3$ and

c -As₂O₃ are isostructures built up by A₄O₆ (A = Sb and As) cages at ambient conditions. Under pressure, it is entirely possible that similar structural transition and amorphization mechanisms exist in compressed α -Sb₂O₃ and c -As₂O₃. The Sb (As) coordination with nearby O in the amorphous phase may have a comparable chemical/coordination environment to those of phase II.

Among the late XV group sesquioxides, pressure-induced amorphization was also observed in α -Bi₂O₃ and β -Bi₂O₃ at high pressure^{48,55}, although their crystal structures are largely different from those of α -Sb₂O₃ and c -As₂O₃ at ambient conditions⁴⁸. Notice that β -Bi₂O₃ is isostructural to phase II of Sb₂O₃⁵⁵. The commonly observed sluggish amorphization process for both cage-like and layered late XV group sesquioxides^{44,45,48,55} indicates an intriguing structural evolution from the long range crystalline order to the short range amorphous order. Thermodynamic calculations and/or spectroscopic experiments will be required to elucidate the underlying amorphization mechanism in late XV group sesquioxides. Also, the effect of the pressure medium on the amorphization remains to be systematically explored.

IV. CONCLUSIONS

In summary, we investigated the high pressure structural and electronic properties of α -Sb₂O₃ up to ~ 50 GPa using neon as the pressure transmitting medium.

The cubic phase I started to transform into a tetragonal phase II at ~ 15 GPa. Besides from variations in local structures and crystal symmetries, these two phases have contrasting electronic properties, seen from the large differences of band gaps and dramatic changes in sample color and transparency. Higher pressure induces a sluggish amorphization process. Our results underscore high pressure as an important tool in exploring the connections between late XV group sesquioxides and understanding their amorphization mechanism.

ACKNOWLEDGMENTS

We thank S. Tkachev, C. Park, S. Sinogeikin, Y. Meng, J. Yan, B. Chen, and A. MacDowell for their assistance. Z. Zhao, Q. Zeng, S. Hirai, and W.L. Mao are supported through the Stanford Institute for Materials and Energy Sciences (SIMES) by the U. S. Department of Energy (DOE), Office of Basic Energy Sciences (BES), under contract DE-AC02-76SF00515. S. Wang is supported by EFree, an Energy Frontier Research Center funded by the DOE-BES under DE-SG0001057. H. Zhang is supported by the Army Research Office, W911NF-09-1-0508. HPCAT operations are supported by DOE-NNSA DE-NA0001974 and DOE-BES DE-FG02-99ER45775, with partial instrumentation funding by NSF MRI-1126249. APS is supported by DOE-BES, under Contract DE-AC02-06CH11357. ALS is supported by DOE-BES under Contract DE-AC02-05CH11231.

* Email: zhaozhao@stanford.edu

- ¹ W. H. Zachariasen, J. Am. Chem. Soc. **54**, 3841 (1932).
- ² A. Byström, Nature **12**, 780 (1951).
- ³ O. Borgen and J. Krogh-Moe, Acta Chem. Scand. **10**, 265 (1956).
- ⁴ C. Wood, B. Van Pelt, and A. Dwight, Phys. Stat. Sol. **54**, 701 (1972).
- ⁵ B. Wolffing and Z. Hurych, Phys. Stat. Sol. **16**, K161 (1973).
- ⁶ C. Svensson, Acta Crystallogr., Sect. B Struct. Sci **30**, 458 (1974).
- ⁷ C. Svensson, Acta. Crystallogr., Struct. Sci. Sect. B **31**, 2016 (1975).
- ⁸ P. S. Gopalakrishnan and H. Manohar, J. Solid State Chem. **15**, 61 (1975).
- ⁹ C. A. Cody, L. DiCarlo, and R. K. Darlington, Inorg. Chem. **18**, 1572 (1979).
- ¹⁰ P. J. Miller and C. A. Cody, Spectrochim. Acta, Part A **38**, 555 (1982).
- ¹¹ A. Datta, A. K. Giri, and D. Chakravorty, Phys. Rev. B **47**, 16242 (1993).
- ¹² J. S. Zabinski, M. S. Donley, and N. T. McDevitt, Wear **165**, 103 (1993).
- ¹³ R. E. de Araujo, C. B. de Araujo, G. Poirier, M. Poulain, and Y. Messaddeq, Appl. Phys. Lett. **81**, 4694 (2002).
- ¹⁴ J. H. Youk, R. P. Kambour, and W. J. MacKnight, Macro-

- molecules **33**, 3594 (2000).
- ¹⁵ A. J. G. Ellison and S. Sen, Phys. Rev. B **67**, 052203 (2003).
- ¹⁶ S. J. Gilliam, J. O. Jensen, A. Banerjee, D. Zeroka, S. J. Kirkby, and C. N. Merrow, Spectrochim. Acta, Part A **60**, 425 (2004).
- ¹⁷ H. Bryngelsson, J. Eskhult, L. Nyholm, M. Herranen, O. Alm, and K. Edström, Chem. Mater. **19**, 1170 (2007).
- ¹⁸ A. Geng, L. Cao, C. Wan, and Y. Ma, Phys. Status Solidi C **8**, 1708 (2011).
- ¹⁹ A. Matsumoto, Y. Koyama, A. Togo, M. Choi, and I. Tanaka, Phys. Rev. B **83**, 214110 (2011).
- ²⁰ A. L. J. Pereira, L. Gracia, D. Santamara-Prez, R. Vilaplana, F. J. Manjón, D. Errandonea, M. Nalin, and A. Beltrán, Phys. Rev. B **85**, 174108 (2012).
- ²¹ E. I. Voit, A. E. Panasenko, and L. A. Zemnukhova, J. Struct. Chem. **37**, 60 (2009).
- ²² R. G. Orman, Phase Transitions in Antimony Oxides and Related Glasses, Thesis for the degree of Master of Science, The University of Warwick, 2005.
- ²³ M. Nalin, Y. Messaddeq, S. J. L. Ribeiro, M. Poulain, V. Briois, G. Brunklaus, C. Rosenhahn, B. D. Mosel, and H. Eckert, J. Mater. Chem. **14**, 3398 (2004).
- ²⁴ M. Nalin, M. Poulain, M. Poulain, S. J. Ribeiro, and Y. Messaddeq, J. Nonklaus, C. Rosenhahn, B. D. Mosel, and H. Eckert, J. Mater. Chem. **14**, 3398 (2004). -Cryst. Solids

- 284**, 110 (2001).
- ²⁵ E. L. Falcao Filho, C. A. C. Bosco, G. S. Maciel, C. B. de Araujo, and L. H. Acioli, *Appl. Phys. Lett.* **83**, 1292 (2003).
 - ²⁶ A. J. Frueh, *Am. Miner.* **36**, 833 (1951).
 - ²⁷ D. Legal and K. Kofifik, *J. Non-Cryst. Solids* **193**, 187 (1995).
 - ²⁸ M. Drache, P. Roussel, and J. -P. Wignacourt, *Chem. Rev.* **107**, 80 (2007).
 - ²⁹ N. M. Sammes and G. A. Tompsett, *J. Eur. Ceram. Soc.* **19**, 1801 (1999).
 - ³⁰ D. Kristallstruktur, *Z. Anorg. Allg. Chem.* **318**, 1762 (1961).
 - ³¹ C. N. R. Rao, G. V. S. Rao, and S. Ramdas, *J. Phys. Chem.* **45**, 672 (1969).
 - ³² S. K. Blower and C. Greaves, *Acta Crystallogr. Sect. C Cryst. Struct. Commun.* **44**, 587 (1988).
 - ³³ A. F. Gualtieri, S. Immovilli, and M. Prudenziati, *Powder Diff.* **12**, 90 (1997).
 - ³⁴ D. Orosel, R. E. Dinnebier, V. A. Blatov, and M. Jansen, *Acta Crystallogr., Sect. B Struct. Sci* **68**, 1 (2012).
 - ³⁵ E. J. Roberts and F. Fenwick, *J. Amer. Chem. Soc* **50**, 2125 (1928).
 - ³⁶ W. B. White, F. Dacheille, and R. Roy, *Z. Krist* **125**, 450 (1967).
 - ³⁷ K. E. Almin and A. Westgren, *Ark. Kemi. Miner. Geol. B* **22**, 15 (1944).
 - ³⁸ I. R. Beatti, K. M. S. Livingstone, G. A. Ozin, and D. J. Reynolds, *J. Chem. Soc. A* **3**, 449 (1970).
 - ³⁹ P. Ballirano and A. Maras, *Z. Krist. NCS* **217**, 177 (2002).
 - ⁴⁰ N. Cornei, N. Tancret, F. Abraham, and O. Mentr, *Inorg. Che* **45**, 4886 (2006).
 - ⁴¹ A. Matsumoto, Y. Koyama, and I. Tanaka, *Phys. Rev. B* **81**, 094117 (2010).
 - ⁴² E. M. Levin and R. S. Roth, *J. Res. Natl. Bur. Stand.* **68A**, 197 (1964).
 - ⁴³ A. Grzechnik, *J. Solid State Chem.* **144**, 416 (1999).
 - ⁴⁴ C. Chouinard and S. Desgreniers, *Solid State Commun.* **113**, 125 (2000).
 - ⁴⁵ E. Soignard, S. A. Amin, Q. Mei, C. J. Benmore, and J. L. Yarger, *Phys. Rev. B* **77**, 144113 (2008).
 - ⁴⁶ S. Ghedia, T. Locherer, R. Dinnebier, D. L. V. K. Prasad, U. Wedig, M. Jansen, and A. Senyshyn, *Phys. Rev. B* **2010**, 024106 (2010).
 - ⁴⁷ T. Locherer, D. L. V. K. Prasad, R. Dinnebier, U. Wedig, M. Jansen, G. Garbarino, and T. Hansen, *Phys. Rev. B* **37**, 214102 (2011).
 - ⁴⁸ A. L. J. Pereira, D. Errandonea, A. Beltrn, L. Gracia, O. Gomis, J. a Sans, B. Garca-Domene, A. Miquel-Veyrat, F. J. Manjn, A. Muoz, and C. Popescu, *J. Phys. Condens. Matter* **210**, 475402 (2013).
 - ⁴⁹ B. H. Toby, *J. Appl. Cryst.* **34**, 210 (2001).
 - ⁵⁰ G. Kresse and D. Joubert, *Phys. Rev. B* **59**, 1758 (1999).
 - ⁵¹ G. Kresse and J. Hafner, *Phys. Rev. B* **47**, 558 (1993).
 - ⁵² J. P. Perdew, K. Burke, and M. Ernzerhof, *Phys. Rev. Lett.* **77**, 3865 (1996).
 - ⁵³ P. Hohenberg and W. Kohn, *Phys. Rev.* **155**, 864 (1964).
 - ⁵⁴ P. E. Blchl, *Phys. Rev. B* **50**, 953 (1994).
 - ⁵⁵ A. L. J. Pereira, R. V. J. A. Sans, O. Gomis, F. J. Manjn, P. Rodriguez-Hernandez, A. Muoz, C. Popescu, and A. Beltrn, *J. Phys. Chem. C* **118**, 23189 (2014).